BIOCHEMISTRY
including biophysical chemistry & molecular biology

Article

pubs.acs.org/biochemistry

# Solution NMR of a 463-Residue Phosphohexomutase: Domain 4 Mobility, Substates, and Phosphoryl Transfer Defect

Akella V. S. Sarma, Asokan Anbanandam,[†] Allek Kelm, Ritcha Mehra-Chaudhary, Yirui Wei, Peiwu Qin, Yingying Lee, Mark V. Berjanskii,[‡] Jacob A. Mick, Lesa J. Beamer,* and Steven R. Van Doren*

Biochemistry Department, 117 Schweitzer Hall, University of Missouri, Columbia, Missouri 65211, United States

Supporting Information

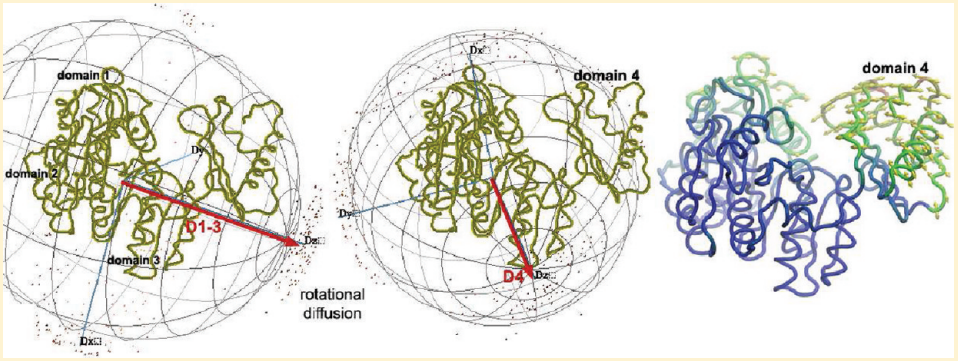


**ABSTRACT:** Phosphomannomutase/phosphoglucomutase contributes to the infectivity of *Pseudomonas aeruginosa*, retains and reorients its intermediate by 180°, and rotates domain 4 to close the deep catalytic cleft. Nuclear magnetic resonance (NMR) spectra of the backbone of wild-type and S108C-inactivated enzymes were assigned to at least 90%. $^{13}C$ secondary chemical shifts report excellent agreement of solution and crystallographic structure over the 14 $\alpha$-helices, C-capping motifs, and 20 of the 22 $\beta$-strands. Major and minor NMR peaks implicate substates affecting 28% of assigned residues. These can be attributed to the phosphorylation state and possibly to conformational interconversions. The S108C substitution of the phosphoryl donor and acceptor slowed transformation of the glucose 1-phosphate substrate by impairing $k_{cat}$. Addition of the glucose 1,6-bisphosphate intermediate accelerated this reaction by 2−3 orders of magnitude, somewhat bypassing the defect and apparently relieving substrate inhibition. The S108C mutation perturbs the NMR spectra and electron density map around the catalytic cleft while preserving the secondary structure in solution. Diminished peak heights and faster $^{15}N$ relaxation suggest line broadening and millisecond fluctuations within four loops that can contact phosphosugars. $^{15}N$ NMR relaxation and peak heights suggest that domain 4 reorients slightly faster in solution than domains 1−3, and with a different principal axis of diffusion. This adds to the crystallographic evidence of domain 4 rotations in the enzyme, which were previously suggested to couple to reorientation of the intermediate, substrate binding, and product release.

$\alpha$-D-Phosphohexomutases from bacteria to humans catalyze reversible transfer of a phosphoryl group across sugar substrates.[1,2] The enzyme phosphomannomutase/phosphoglucomutase (PMM/PGM) from the opportunistic human pathogen *Pseuodomonas aeruginosa* converts phosphorylation between positions 1 and 6 of either mannose or glucose. The reaction proceeds between hexose 1-phosphate, its phosphorylation to hexose 1,6-bisphosphate, and rephosphorylation of the enzyme to generate the hexose 6-phosphate (Figure 1).[3] Retention of the bisphosphorylated intermediate during catalysis was demonstrated by isotope trapping.[1,4] That, together with the opposite orientations of glucose 1-phosphate (G1P) and glucose 6-phosphate (G6P) in crystal structures[5] and conservation of Ser108 required for activity[6] and implicated in donating and accepting the phosphoryl group,[3] strongly suggests the reorientation of the glucose 1,6-bisphosphate (G1,6P) intermediate by 180° on the enzyme. Moreover, the bound G1,6P forms either G1P or G6P 14−15 times more often than this intermediate dissociates.[4] Crystallography confirmed the proposed roles of Ser108 and provided insights into how the intermediate is reoriented by 180° in the active site.[5,7]

In *P. aeruginosa*, the G1P product is used in biosynthesis of the nucleotide-activated UDP-D-glucose and dTDP-L-rhamnose precursors of the lipopolysaccharide (LPS) core required for virulence.[8] dTDP-L-rhamnose is also a precursor of rhamnolipids that are surfactants associated with biofilms of *P. aeruginosa*.[9] The mannose 1-phosphate product is used in the biosynthesis of the GDP-D-mannose precursor to the LPS A-band[10] and the alginate capsule[11] that protects the bacterial communities from antibiotics and phagocytosis.[12] PMM/PGM

**Received:** October 20, 2011
**Revised:** December 14, 2011
**Published:** January 5, 2012

  

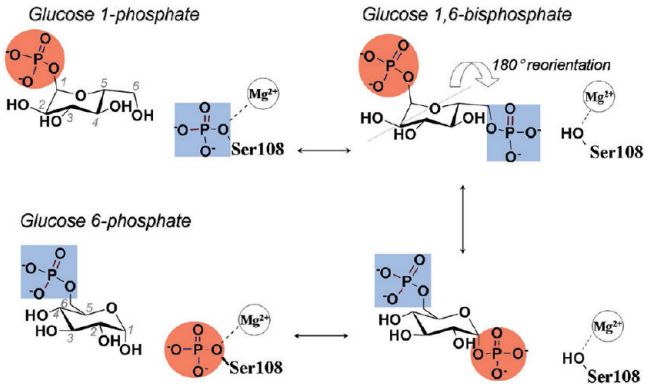


**Figure 1.** Steps of transformation of G1P to G6P by α-D-phosphohexomutases. The reversible catalysis proceeds via the G1,6P intermediate that is reoriented by 180° on the enzyme. A red circle marks the phosphoryl group transferred from position 1 to Ser108 of *P. aeruginosa* PMM/PGM. Not depicted is the infrequent dissociation of G1,6P.

is a potential target for antibiotic development because *P. aeruginosa* infections accompany cystic fibrosis[12,13] and severe chronic obstructive pulmonary disease.[14] Because the related rabbit PGM has a 6000-fold preference for glucose over mannose phosphosugars[15] while bacterial PMM/PGM enzymes have specificity for both, mannose-like compounds were suggested as a potential strategy for inhibiting only bacterial enzymes.[5]

Bacterial PMM/PGM comprises four mixed $\alpha/\beta$-domains encompassing a deep and positively charged catalytic cleft.[16] The first three domains share a common fold of a four-stranded $\beta$-sheet between two helices.[16] Domain 4 is topologically distinct and is classified as a member of the TATA-box binding protein-like superfamily.[17] Upon binding a phosphosugar ligand such as G1P, G6P, or xylose 1-phosphate (X1P), domain 4 (D4) closes inward to narrow the catalytic cleft, indicating that D4 can reorient.[5,7,18] (X1P is an inhibitor and analogue of G1P that lacks C6 and the O6 hydroxyl, rendering it incapable of phosphoryl transfer.) Binding of the hexose substrate or the accompanying conformational change is rate-limiting for PMM/PGM.[4] A network of hydrogen bonds between the ligand and several loops in the active site, combined with favorable electrostatics, positions the bound ligand deep in the pocket.[5,7] During the multistep reaction, partial opening of the catalytic cleft by rotation of D4 might facilitate the requisite 180° flip of the G1,6P or mannose 1,6-bisphosphate (M1,6P) intermediate,[7] which is retained in the active site presumably with the aid of the electrostatic field.[7,16]

NMR in solution can in principle address issues like the rotational diffusion of domains, protein fold, transformation of substrate, consequences of a key mutation, internal dynamics, heterogeneity, protein stability, and phosphosugar binding. The first six of these topics are addressed in part in this work. We removed the key phosphoryl donor and acceptor via an S108C substitution in an effort to simplify the future study of ligand binding, with the hope of preventing chemical transformation while retaining coordination of the divalent cation in the active site. Despite the challenging size of 51 kDa, assignments of the backbone NMR peaks of wt PMM/PGM as well as effects of the S108C substitution of the key phosphoryl donor and acceptor have been determined. NMR in solution suggests (i) detectably greater mobility of D4 than D1−D3 as rigid bodies (by $^{15}$N $R_1/R_2$ and $\eta_{xy}$ relaxation and NMR peak heights), (ii) the presence of conformational substates affecting one-fourth of the residues (in TROSY-resolved spectra), and (iii) potential mobility in milliseconds of four loops that interact with phosphosugar ligands (based on $^{15}$N relaxation and peak heights). NMR and crystallography indicate perturbations due to the S108C substitution are distributed around the catalytic cleft. The ability of G1,6P to partially restore the catalytic defect from the S108C substitution suggests alternative means of phosphoryl transfer between the enzyme and hexose. Thus, this active site cleft displays evidence of resilience to a strategic mutation and adjustable shaping of the cleft as D4 reorients.

## EXPERIMENTAL PROCEDURES

**Protein Expression, Isotopic Enrichment, and Purification.** The S108C mutation of *P. aeruginosa* PMM/PGM was constructed in pET3a using the QuikChange mutagenesis kit (Stratagene) and verified by DNA sequencing. For expression of uniformly $^{2}$H-, $^{15}$N-, and $^{13}$C-labeled PMM/PGM, *Escherichia coli* BL21(DE3) cells were transformed with either a pET14b or pET3a expression plasmid, corresponding to either the $His_6$-tagged or untagged protein, respectively. Starter cultures grown overnight were centrifuged, and the cell pellet was added to 30 mL of fresh M9 minimal medium containing $^{15}NH_4Cl$, [$^{13}$C]glucose (Sigma-Isotec), 0.1 mg/L carbenicillin, and 5% (v/v) [$^{13}$C,$^{15}$N]Celtone (Cambridge Isotope Laboratories) and grown to an $OD_{600}$ of 0.6−0.8. The cell pellet from this culture was added to 200 mL of the same medium prepared in $D_2O$, grown to an $OD_{600}$ of 0.6−0.8, and then added to 1 L of the same medium, resulting in a $D_2O$ concentration of 93% (v/v). Cells were grown to an $OD_{600}$ of 0.6−0.8, induced by addition of IPTG to a final concentration of 0.4 mM, and grown at 37 °C for 4−6 h until they were harvested. Cell pellets were stored at −80 °C.

Purification of $His_6$-tagged samples was performed as described previously[19] with modifications. The cells were lysed with a French press in buffer for equilibrating the $Ni^{2+}$ column [20 mM sodium phosphate (pH 7.8), 300 mM NaCl] containing 14 mM $\beta$-mercaptoethanol, 2 mM $MgSO_4$, 2 mM $CaCl_2$, 0.5 mM PMSF, 0.5 mM TLCK, and 10 μg/mL DNase. The thiol reductant was present to keep the one exposed and six buried cysteine sulfhydryls reduced. The supernatant was treated with protamine sulfate (5 mg/g of cell pellet), centrifuged, and then mixed with $Ni^{2+}$ affinity resin (Sigma, His-Select). Protein was eluted using buffer with 250 mM imidazole (pH 7.8) added. The purified protein was dialyzed against 20 mM phosphate (pH 7.4) into successively lower NaCl concentrations of 300, 200, and 100 mM, then into 50 mM MOPS (pH 7.4) at 50 and 25 mM NaCl, and finally into 50 mM MOPS (pH 7.4) with 1 mM $MgCl_2$. Dephosphorylation of a sample was achieved by overnight incubation with glucosamine 1-phosphate at a 6.25:1 molar excess over enzyme at 4 °C (Y. Lee and L. J. Beamer, unpublished observations), followed by thorough dialysis in 50 mM MOPS (pH 7.4) and 1 mM $MgCl_2$.

Untagged protein was purified as described previously,[3] via cell lysis with a French press. This protein was also dialyzed into 50 mM MOPS (pH 7.4) either with or without 1 mM $MgCl_2$. Protein solutions were concentrated to 40−75 mg/mL as determined with a Bradford assay. A typical yield from 1 L of culture was 70−100 mg of purified protein.

**NMR Spectra and Assignment.** NMR spectra were acquired with a Bruker Avance III 800 MHz spectrometer with a TCI cryoprobe. PMM/PGM samples were at


dx.doi.org/10.1021/bi201609n | *Biochemistry* 2012, 51, 807−819

concentrations of 0.6−1.5 mM in the pH 7.4 buffer described above. HNCA, HN(CO)CA, HNCO, HN(CA)CO, HNCACB, and HN(CO)CACB triple-resonance spectra at 37 °C exploited TROSY line sharpening[20] for sensitivity and resolution.[21,22] $^{1}$H and $^{13}$C peak assignments were referenced directly to DSS and indirectly to $^{15}$N.[23] NMR spectra were processed with NMRPipe[24] or TopSpin and interpreted with Sparky.[25] Sequence placement of peak assignments exploited residue-specific information from seq_prob,[26] MARS,[27] and SAGA.[28] In cases where corresponding amide peaks from different triple-resonance spectra were not recognized by SAGA as matching, the generic spin system was manually edited into the .gs file. This maximized successful SAGA assignments and confirmation of spin systems.

**Structural Information from NMR.** Secondary structure propensities were derived from $^{13}C\alpha$ and $^{13}C\beta$ shifts from random coil, scaled from +1.2 to −1.2, and averaged over a sliding five-residue window.[29] This SSP algorithm has the advantage of simplifying secondary structural trends by normalizing the scales of $^{13}$C chemical shift changes to a uniform scale shared by all types of amino acids, which otherwise differ in the size of the changes.[29]

The CS23D webserver[30] was used to build a model of the free state of PMM/PGM refined by assigned chemical shifts. The final refinement step of CS23D was modified to allow the chemical shifts to drive refinement and to prevent collapse of D4 against D1. That is, the knowledge-based potential was turned off, and the secondary structure was loosely restrained to a 1 Å root-mean-square deviation (rmsd) from the starting model.

**$^{15}$N NMR Relaxation.** $^{15}$N $T_1$, $T_2$, and $\{^1H\}^{15}N$ steady-state NOE relaxation were measured on the 800 MHz NMR spectrometer using TROSY-T1, TROSY-T2, and NOE-TROSY pulse sequences, respectively, with enhanced $^{1}$H resolution and sensitivity.[31] The $T_1$ and $T_2$ series were each run with the various relaxation periods collected in an interleaved fashion. $T_1$ relaxation periods were 0.05, 0.21, 0.49, 0.85, and 1.3 s. $T_2$ relaxation periods were 0, 16, 32, and 48 ms. Saturated and unsaturated $\{^1H\}^{15}N$ NOE spectra were collected in an interleaved manner. Three replicate pairs of them were collected. Six seconds was used for either $^{1}$H saturation or recovery in the unsaturated reference spectra. Rate constants $\eta_{xy}$ of $^{15}$N DD-CSA transverse cross-correlated relaxation were measured as described previously[32] on the Bruker 800 MHz system.

Mean $R_2/R_1$ ($=T_1/T_2$) and mean $\eta_{xy}$ values were used to estimate apparent rotational correlation times $\tau_c$ after trimming off the highest 10% and lowest 10% of values that can be subject to internal motions. $\tau_c$ was estimated from trimmed mean $T_1/T_2$ using the relationship[33]

$$\tau_c = \frac{1}{2\omega_c}\sqrt{\frac{6T_1}{T_2} - 7} \quad (1)$$

Trimmed means of $\eta_{xy}$ were used to estimate $\tau_c$ from spectral density relationships of the TRACT approach.[34] To model the orientation properties of rotational diffusion, the trimmed $^{15}$N $R_2$ and $R_1$ relaxation rates were fitted to the coordinates of the free state of wt PMM/PGM [Protein Data Bank (PDB) entry 1K35] using TENSOR2.[35] F testing was used to identify the simplest model of diffusion that is statistically adequate.

**Transfer of a Phosphoryl Group across Glucose.** Both one-dimensional $^{1}$H and $^{13}$C spectra were used to monitor transformation of $^{13}$C-labeled G1P (Cambridge Isotope Laboratories, Andover, MA) to G6P by 33 μM PMM/PGM at 27 °C and pH 7.3. The initial reaction mixture contained 400 μM G1P, 1 mM $MgSO_4$, 1 mM DTT, 33.3 mM Tris-$d_{11}$, and 16.7 mM MOPS (pH 7.3), with the addition of G1,6P to a final concentration of 0.66 μM. DTT (1 mM) was previously found necessary for optimal activity.[3] The relative concentrations of G1P and G6P were derived by integrating the $^{1}$H NMR peak of the α-anomeric proton of each, which lie at 5.44 and 5.22 ppm, respectively. (The β-anomeric peak overlaps with the suppressed water region.) The finding via $^{13}$C NMR of 1.67-fold more β-anomer was used in determining the total concentration of G6P ($[G6P]_{total}$) formed. That is, in $^{1}$H spectra, $[G6P]_{total} = (1.67 + 1)[G6P]_{\alpha\text{-anomer}}$.

Enzymatic progress curves and initial velocities were monitored in the direction of G6P formation using an assay coupled with glucose-6-phosphate dehydrogenase that reduces $NAD^+$ to NADH detected by its absorbance at 340 nm.[3] The reactions were conducted at 25 °C in 50 mM MOPS (pH 7.4) with 1 mM DTT, 1.5 mM $MgSO_4$, 0.9 mM $NAD^+$, 1−1.5 μM G1,6P, and 100−200 nM (5−10 μg/mL) PMM/PGM.

**Mass Spectrometry.** Enzyme samples were diluted in a 3:97:0.1 (v/v/v) acetonitrile/water/88% formic acid mixture and analyzed by NanoLC-Nanospray QTOF MS (Agilent 6520A MS) (with a mass error of <5 ppm) in positive ion mode. Fractionation was conducted with an Agilent SPQ 105 Intact Protein Chip with a Zorbax C8 trap column. Spectral deconvolution used maximum entropy implemented with Agilent Mass Hunter.

**Circular Dichroism.** Protein samples were dialyzed into 10 mM MOPS (pH 7.4). The dialysate was used as the reference for background subtraction. CD spectra were recorded using an Aviv model 62DS spectrometer over wavelengths from 200 to 250 nm at 25 °C in a cuvette with a path length of 0.1 cm.

**Crystallography.** The free state of PMM/PGM(S108C) was crystallized as described previously[36] with a final solution containing 25% glycerol as a cryoprotectant, 0.1 M HEPES (pH 7.5), and 1.4 M K/Na tartrate. X-ray diffraction data were collected using a Rigaku RU H3R rotating anode and R-AXIS IV$^{++}$ image plate system under cryo-cooling conditions. Data were processed with d*Trek,[37] and refinement was performed with REFMAC version 5.5.0109.[38] The starting model for refinement of the apo-S108C crystals was that of wt apo-PMM/PGM (PDB entry 1K35) without water molecules. The progress of the refinement was monitored by following $R_{free}$; 5% of the data set was set aside for cross-validation prior to refinement. The structure was refined to convergence through iterative cycles of refinement and manual rebuilding with Coot.[39] Water molecules were placed automatically with COOT in peaks of >3.0σ in $F_o - F_c$ maps and within reasonable hydrogen bonding distance of oxygen or nitrogen atoms. The data collection and refinement statistics are summarized in Table 1.

**Statistics of Conformational Change.** Multivariate statistics were used to recognize patterns of conformational change in crystal structures. Principal component analysis (PCA) of the covariance in coordinates[40] was implemented with the ProDy package.[41] PCA was applied to 12 structures of *P. aeruginosa* PMM/PGM, comprising three open and unbound structures (PDB entries 1K35, 1K2Y, and 3C04), the half-closed enzyme bound to G1,6P (PDB entry 2FKF), and eight closed, ligand-bound structures (PDB entries 1P5D, 1P5G, 1PCJ, 1PCM, 2H5A, 2H4L, 2FKM, and 3BKQ). Only Cα

**Table 1. Crystallographic Data for PMM/PGM(S108C)**

| | |
|---|---|
| Data Collection | |
| X-ray source | Home |
| space group | $P2_12_12_1$ |
| unit cell dimensions (Å) | $a$ = 70.03, $b$ = 72.81, $c$ = 93.0 |
| $\lambda$ (Å) | 1.54 |
| resolution (Å) (outermost shell) | 57.33−2.10 (2.18−2.10) |
| no. of unique reflections | 28767 |
| redundancy | 4.80 (4.72) |
| $R_{merge}$ (%) | 6.0 (51.3) |
| $I/\sigma$ | 11.0 (2.3) |
| completeness (%) | 99.9 (99.9) |
| Refinement | |
| resolution (Å) | 57.35−2.10 |
| $R_{work}$ [a]/$R_{free}$ [b] | 21.3/25.3 |
| no. of non-H atoms | 3402 |
| waters | 116 |
| $B$ value from the Wilson plot (Å$^2$) | 46.1 |
| $\langle B \rangle$ (Å$^2$) | |
| protein atoms | 56.3 |
| waters | 57.4 |
| phosphate ion | 56.2 |
| rmsd for bonds (Å)/angles (deg) | 0.012/1.4 |
| Ramachandran (%) | |
| most favored | 94.3 |
| allowed | 4.3 |

[a] $R_{work} = \sum||F_o| - |F_c||/\sum|F_o|$, where $F_o$ and $F_c$ are the observed and calculated structure factors, respectively. [b] $R_{free}$ is the $R$ factor calculated from 5% of the reflections not included in refinement. No $\sigma$ cutoff of the data was used.

coordinates were used, thereby avoiding complication by point mutations or missing side chain coordinates. The directions and relative amplitudes of the statistical change in C$\alpha$ coordinates were displayed for the main modes (principal components or PCs) using the NMWiz plugin for VMD.[41]

## RESULTS

**Assignments of Triple-Resonance NMR Spectra.** The amide peaks of PMM/PGM TROSY spectra are sufficiently resolved at 800 MHz to permit sequential assignments despite the crowding and overlap in the central region (Figure 2). Assignment of backbone NMR peaks of $^2$H-, $^{13}$C-, and $^{15}$N-labeled PMM/PGM with a His tag commenced using 800 MHz TROSY-enhanced HNCA, HN(CO)CA, HNCO, HN(CA)-CO, HNCACB, and HN(CO)CACB spectra of proven utility in assigning larger enzymes.[21,22,42] Sequential assignments of ~170 amide peaks were obtained with the aid of MARS.[27] Manual interpretation doubled the number of preliminary assignments to 333 amide spin systems. Assignments of D4, which has greater peak heights, were complete at this stage. However, large gaps in assignments remained in D3, as well as many small gaps across D1 and D2. Another sample of $^2$H-, $^{13}$C-, and $^{15}$N-labeled wt PMM/PGM prepared without the His tag and with 1 mM $MgCl_2$ displayed slightly sharper and more peaks, with peak positions unaltered. A battery of triple-resonance spectra of this 1 mM sample [lacking an HN(CO)-CACB] supported manual assignments that reached 403 of 437 potentially assignable amide spin systems. A battery of the same five TROSY-enhanced triple-resonance spectra was collected on a 0.75 mM sample of $^2$H-, $^{13}$C-, and $^{15}$N-enriched, S108C-substituted PMM/PGM in 1 mM $MgCl_2$. Manual peak assignments started from those of the wt enzyme.

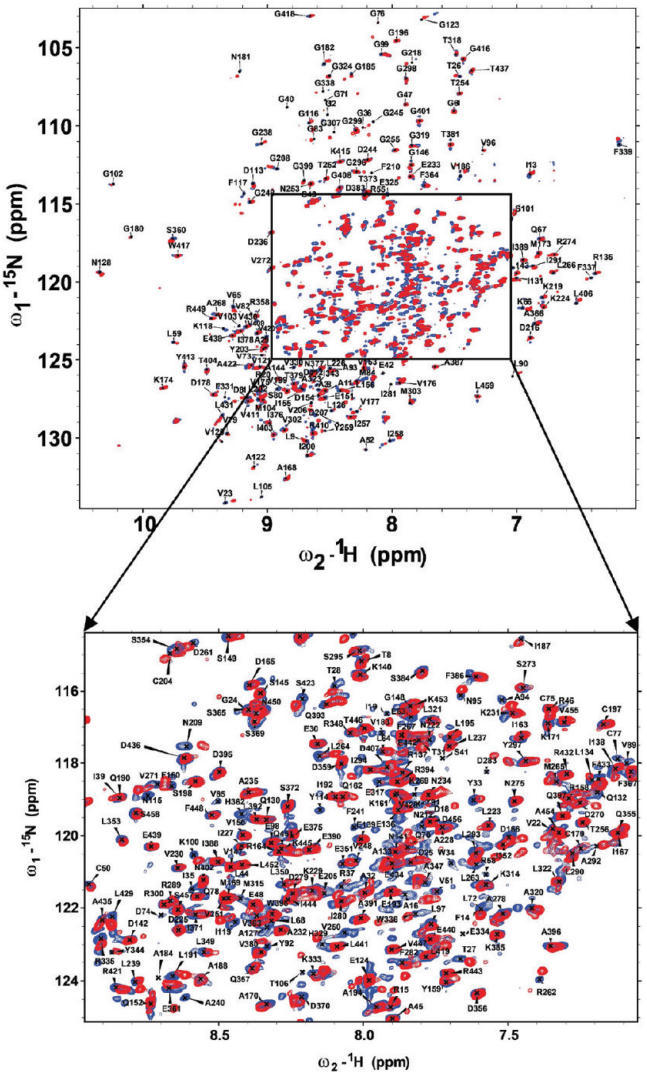


**Figure 2.** Annotated TROSY spectra of perdeuterated wt PMM/PGM (red) and PMM/PGM(S108C) (blue) at 800 MHz, 37 °C, and pH 7.4.

The accuracy of the peak assignments was confirmed by applying SAGA automation developed for larger proteins.[28] This confirmed 401 of the prior triple-resonance spin systems of the wt enzyme, adjusted peak assignments of two spin systems, and identified a few new assignments. Most of the resonances that remain unlabeled in Figure 2 lack triple-resonance correlations needed to assign them. Peak assignments of the termini, short stretches between prolines, and loops especially in D3 with presumed line broadening remain in doubt. In the case of PMM/PGM(S108C), SAGA confirmed the peak assignments of 372 residues, corrected the chemical shifts of five more, and assigned 16 additional spin systems. Pivotal to successful assignments by SAGA was the completeness of its assembly of generic spin systems (GSs) from the lists of peaks picked from the triple-resonance spectra. Several dozen expected GSs failed in part or in full to reach SAGA's step of assigning peaks. At least part of the omissions stemmed from SAGA curation of peak lists failing to match triple-resonance peaks to the corresponding peak in the HN(CO)CA reference list. This resulted in "rungs" ($^{13}$C


dx.doi.org/10.1021/bi201609n | Biochemistry 2012, 51, 807−819

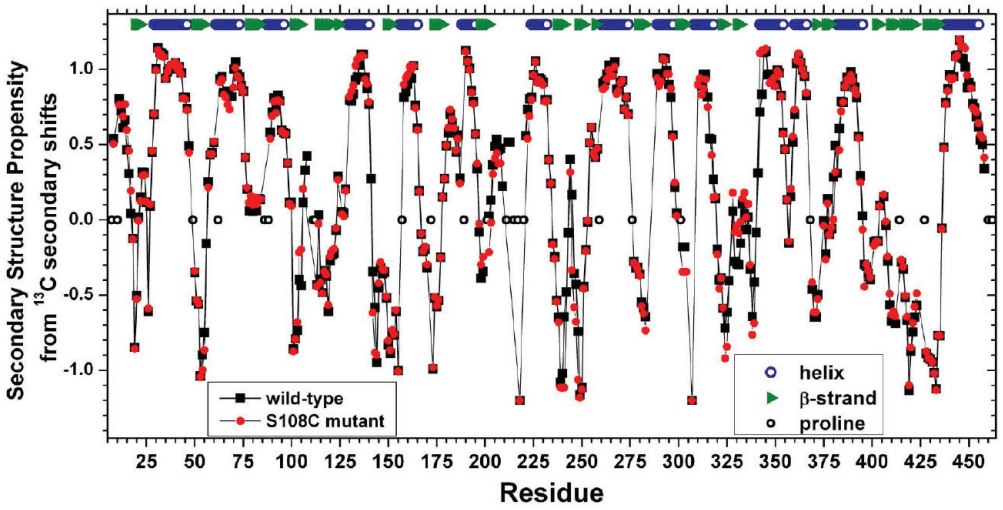


**Figure 3.** Secondary structure propensities (SSPs) from $^{13}C\alpha$ and $^{13}C\beta$ secondary chemical shifts. SSP values are indicated for the wt enzyme (black squares) and the S108C-substituted enzyme (red circles). The values were calculated over a sliding window of five residues, avoiding glycine and each residue prior to proline.[29] $^{13}$C was referenced to DSS. The locations of secondary structure in crystal structures[16] are marked at the top for comparison with SSP trends in solution.

peaks for sequential connection) missing from GSs. Manual grouping of triple-resonance peaks into ~100 GSs filled in the critical omissions. Upon addition of the hand-assembled GSs and removal of incomplete GSs having four or more missing rungs, completion of assignments by SAGA became excellent. Among 437 potential amide spin systems, 407 (93%) of those of wt PMM/PGM and 393 (90%) of those of PMM/PGM(S108C) were assigned and confirmed (Figure 2).

**Structural Correlates of NMR Secondary Shifts.** $^{13}C\alpha$ and $^{13}C\beta$ secondary chemical shifts can be normalized to highlight secondary structure propensity (SSP).[29] Across 20 of the 22 $\beta$-strands, SSP values were $\leq$0.15 (Figure 3). High SSP values of 0.57−1.2 show excellent correspondence with the locations of the 14 $\alpha$-helices in crystal structures (Figure 3). In three helices, the C-terminal residue has a lower SSP value of 0.40 at Glu233, 0.27 at Thr318, and 0.03 at Asp395. Each of these and Tyr297 with an SSP of 0.57 is the C-cap position of the hydrophobic C-capping motif distinguishing that helix. Using established nomenclature,[43] the helix ending at Glu233 has a $C^{4\prime} \rightarrow$ C3 n (type V or non-Gly Schellman) cap. The helix ending at Thr318 has a $C'' \rightarrow$ C3/C′ Gly (type IV or Schellman) cap. The helix ending at Asp395 has a $C^{3\prime} \rightarrow$ C3/C′ n (type Va or non-Gly Schellman) cap. The helix ending at Tyr297 has the less common C4′ → C3 Gly (type VIb) cap.

The assigned NMR chemical shifts were used to refine a homology model from a torsion-based genetic algorithm with modifications to refinement listed in Experimental Procedures.[30] The model is superimposed with the crystal structure of the free state of PMM (PDB entry 1K35) in Figure 4 with a backbone rmsd of 1.29 Å. All 14 helices and 22 $\beta$-strands are present in the NMR-refined model and correspond well in location with those of the crystal structure, except for a few $\beta$-strands in D1−D3 that appear to be longer in the NMR-refined model. As the structural information from $^{13}C\alpha$ and $^{13}C\beta$ NMR secondary chemical shifts is localized to the backbone, it cannot itself define the relative orientation of the domains. Superposing each domain individually between the solution model and the crystallographic coordinates yielded backbone rmsd values of 0.60 Å for D1 (residues 9−154), 0.38 Å for D2 (residues 155−258), 1.01 Å for D3 (residues 259−367), and 0.62 for D4 (residues 368−463).

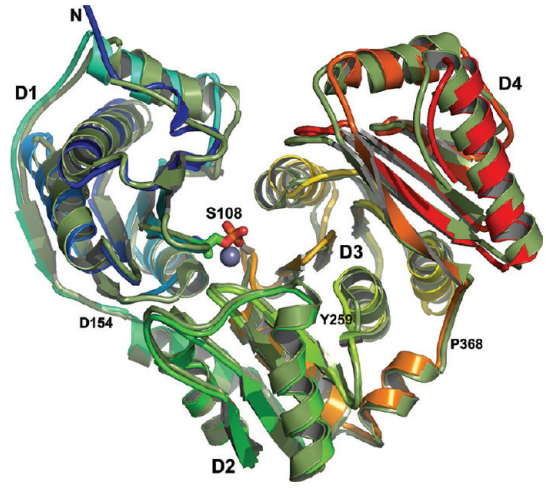


**Figure 4.** NMR chemical shift-refined homology model of PMM/PGM superimposed on the crystal structure. The solution NMR-enhanced model is colored the spectrum of the rainbow from blue at the N-terminus to red at the C-terminus. The crystal structure of the free state (PDB entry 1K35)[16] is colored green. The side chain of phospho-Ser108 is drawn at the base of the catalytic cleft where its O$\gamma$ is one ligand of the metal ion[16] (gray and presumed to be zinc). Loop junctions between domains are marked with residue numbers.

**NMR Evidence of Substates.** Approximately 115 amide groups of wt or S108C-substituted PMM/PGM have two recognizable peaks in 800 MHz TROSY and triple-resonance spectra. These residues are distributed throughout D1−D3 and on the face of D4 adjacent to D3 (Figure 5). Key active site residues able to contact bound ligand such as Arg20, Lys118, and Arg247 are affected. Three residues (Leu266, Val272, and Ser273) of the central helix of D3 each have three peaks resolved, while Asn128 of D1 facing D3 has four. Examples with two peaks are depicted in Figure S1 of the Supporting Information. Chemical shift differences between major and minor peaks are given in Figure S2 of the Supporting Information. The minor peak is always smaller in TROSY


dx.doi.org/10.1021/bi201609n | *Biochemistry* 2012, 51, 807−819

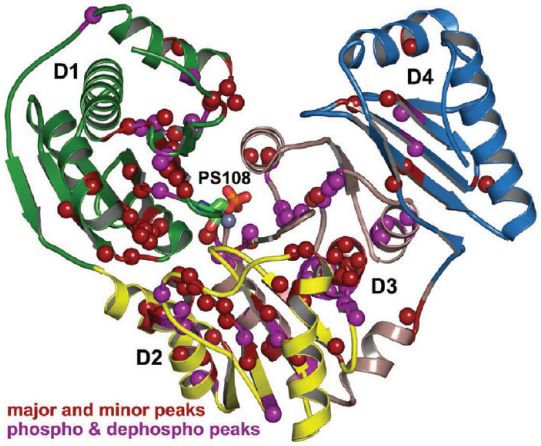


**Figure 5.** Residues with major and minor peaks, suggesting substates. Residues with two amide correlations resolved are marked with spheres. Purple spheres mark amide groups for which the minor peak represents the dephosphorylated wt enzyme (see Figure S2 of the Supporting Information). Dark red spheres mark the other amide groups having major and minor peaks. D1–D4 are colored green, yellow, pink-gray, and sky blue, respectively.

spectra. However, for ~28 residues of wt PMM/PGM, the minor peak dominates triple-resonance (Figure S1 of the Supporting Information) and $^{15}$N relaxation spectra, suggesting that it relaxes more slowly than its fast-relaxing major counterpart.

The preparation of wt PMM/PGM in a mostly dephosphorylated state (>90% based on mass spectra not shown) resulted in the usual major peak of ~43 residues nearly disappearing and being replaced by the usual minor peak (Figure S2 of the Supporting Information). Consequently, the major peak is assigned to the phosphorylated state and the minor peak to the dephosphorylated state for these 43 residues. Though the S108C mutant appears to be completely dephosphorylated (Figure S3 of the Supporting Information), it still has ~114 amide groups with major and minor resonances (Figure S2 of the Supporting Information). Among the 72 amide groups of the wt enzyme with two peaks not obviously affected by phosphorylation (Figure S2 of the Supporting Information), ~30% have elevated $^{15}$N $R_2$ or $R_2/R_1$ evidence of exchange broadening (Figure 7a,b). This suggests the possibility of underlying conformational exchange processes that overlap the millisecond scale for the residues affected.

**Domain 4 Mobility.** The relative mobility of domains of larger proteins can be judged qualitatively by peak heights of TROSY-enhanced triple-resonance spectra, which are sensitive to correlation times of overall rotational diffusion and to faster, localized dynamics.[44] D4, on the whole, has greater peak heights than the other domains. In TROSY-enhanced HNCO spectra, peak heights from D4 are on average 2.1-fold higher than those from D1–D3 for wt PMM/PGM (Figure 6a) and 2.25-fold higher for PMM/PGM(S108C) (Figure 6b). This suggests that D4 rotationally reorients as a rigid body more quickly than D1–D3.

$^{15}$N NMR relaxation was measured to examine this hypothesis further. $^{15}$N relaxation parameters $R_2$, $R_2/R_1$, $\eta_{xy}$, and $\{^1H\}^{15}N$ NOE each are decreased starting immediately after D3–D4 hinge residue Pro368 through the first third of D4 (Figure 7). $^{15}$N $R_2/R_1$ and $\eta_{xy}$ parameters are favored for analyzing hydrodynamics.[33−35] The averages of $R_2/R_1$ and $\eta_{xy}$ over the first third of D4 are 78 and 82%, respectively, of their averages over D1–D3. Part of these decreases can be attributed to localized motions in the first third of D4 as pointed out below. Over the remaining two-thirds of D4, $R_2/R_1$ averages 91% of the D1–D3 average and $\eta_{xy}$ averages 95% of its D1–D3 average (Figure 7b,c). The trimmed mean $R_2/R_1$ of 64.0 for D1–D3 implies an apparent rotational correlation time $\tau_c$ of ~19.0 ns using eq 1, while the trimmed mean $R_2/R_1$ of 56.0 for all of D4 implies a $\tau_c$ of ~17.8 ns, which is 6.7% shorter. Fits of the same sets of $^{15}$N $R_2$ and $R_1$ relaxation rates using TENSOR2[35] also place $\tau_c$ at 19.0 ns for D1–D3 and 17.8 ns for D4. At the lower temperature of 35 °C, trimmed mean $^{15}$N $\eta_{xy}$ values (Figure 7c) interpreted by the TRACT method[34] suggest an apparent $\tau_c$ for D1–D3 of 21.2 ns and a $\tau_c$ for D4 of 19.0 ns, which is 10% shorter. At 37 °C, PMM/PGM(S108C) displays a similar $\tau_c$ of 20.3 ns for D1–D3 and a $\tau_c$ of 18.8 ns for D4 based on $^{15}$N $\eta_{xy}$ values shown in Figure S6 of the Supporting Information. These correlation times imply that each sample was a monomer in which D4 appeared to reorient rotationally 6–10% faster than D1–D3.

The diffusion tensors of D1–D3 and D4 were simulated in TENSOR2[35] using the trimmed $^{15}$N $R_2$ and $R_1$ values (from Figure 7). F testing established that the simplest statistically adequate diffusion tensors have the axial symmetry of prolate ellipsoids. The best fit to D1–D3 has a $D_\parallel/D_\perp$ of 1.14. The best fit to D4 has a $D_\parallel/D_\perp$ of 1.24. Notably, the direction of the principal axis of diffusion for D1–D3 ($D_\parallel$ or $D_z$) differs from that of D4 by roughly 55°, which is beyond experimental uncertainty (Figure S7 of the Supporting Information). This bolsters the line shape evidence of the partial independence in the rotational diffusion of D4.

Addition of a saturating level of X1P decreased average peak heights of D4, which are 1.3-fold higher than those of D1–D3 for the wt enzyme (Figure 6a) and 1.95-fold greater for the S108C-substituted enzyme (Figure 6b). The higher overall peak heights of D4 remaining with X1P bound raise the question of whether D4 still reorients more quickly in the inhibitor complex, in a subtle but detectable fashion, particularly with PMM/PGM(S108C). The possible nature and significance of the rotation of D4 are considered in Discussion.

**Mobile Loops.** Mobility within the domains is also suggested by locally varying NMR peak heights and $^{15}$N relaxation. Greater peak heights, consistent with internal motions within nanoseconds, map to a number of locations, including loops and surface locations of the enzyme (Figure 6). The most obvious of the rapidly mobile loops apparent from tall peaks are distant from the active site. Two of these flank the boundary defined between D1 and D2, encompassing a loop and final $\beta$-strand of D1 (Asp142–Asp154) and a loop following the first helix of D2 (Ala168–Met173) (Figure 6). Another rapidly mobile loop is found just after the final helix of D3. Highly flexible loops terminate both ends of the first helix of D4 (Figure 6). These latter three loops are near the "hinge" region, a noted site of conformational change at the juncture of D3 and D4 around Pro368.[7,45] All five of these loops have instances of below average $^{15}$N $R_2$ and $\eta_{xy}$ values that confirm the peak height evidence of fast motions within nanoseconds (Figure 7a,c). These loops, except for Asp142–154, also have low $\{^1H\}^{15}N$ NOE values (Figure 7d) that further suggest the presence of motions on the picosecond scale.

At each loop that can make contacts with phosphosugar ligands,[5,7] residues are found with locally smaller amide peak

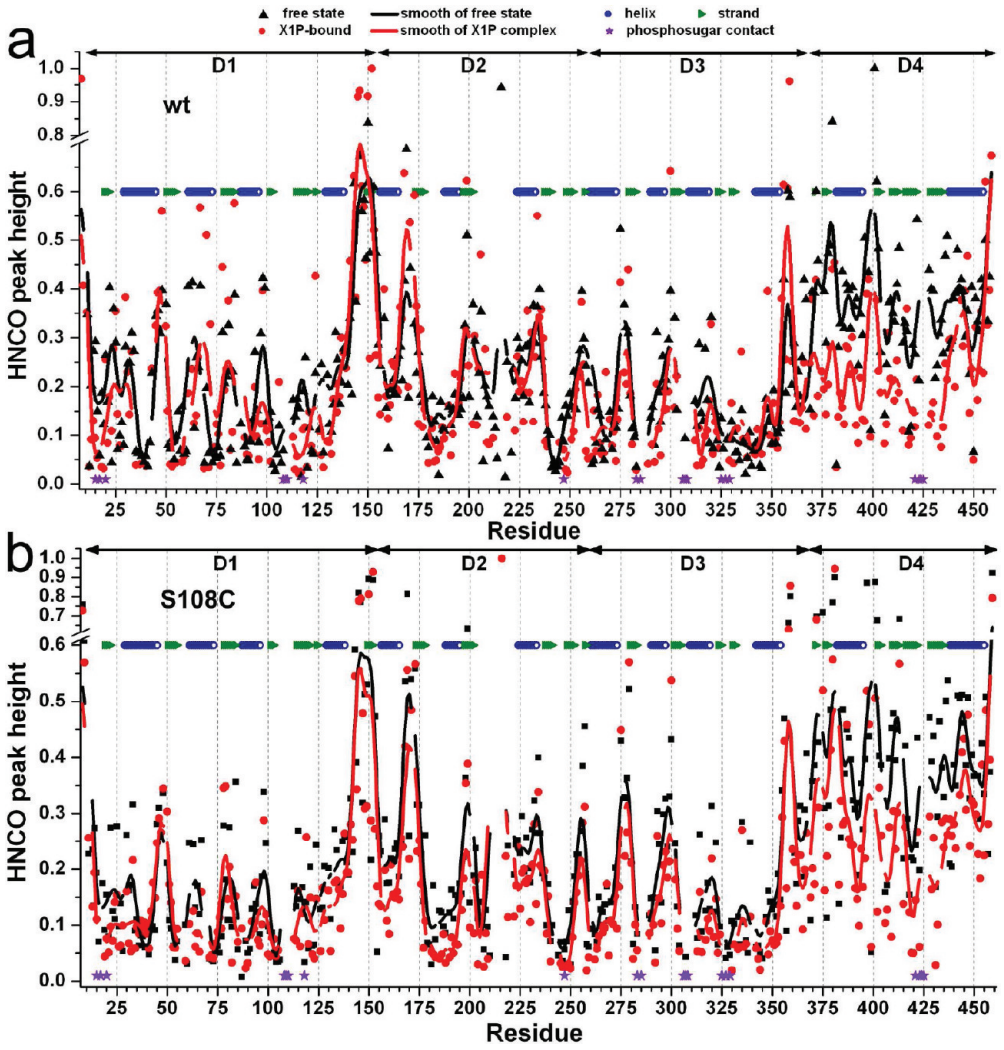


**Figure 6.** NMR evidence of mobility of D4 and loops. Peak heights of TROSY-enhanced HNCO spectra, normalized to the tallest peaks, are plotted for wt PMM/PGM (a) and PMM/PGM(S108C) (b), both before (black) and after saturating addition of X1P to a 5-fold molar excess (red). Domain boundaries are marked at the top. Curves indicate smoothing by three-point fast Fourier transformation that filtered out extremes in peak heights. Sequence positions that contact phosphosugars are marked with purple stars.

heights; these are resolved and compared by TROSY-HNCO and marked with purple stars in Figure 6. This list includes Arg15, Tyr17*, Arg20, Ser108, Lys118, Arg247, Asp283, Gly307*, Glu325, Ser327, His329*, Arg421, and Ser423 that contact ligands. Each asterisk marks an amide proton that could be subjected to the potential broadening mechanism of exchange with the water solvent at 1−5 $s^{-1}$ (not shown). However, the short or missing peaks of the 10 other residues might possibly be attributable to line broadening from fluctuations within milliseconds. This is corroborated in four of these loops by $^{15}N$ exchange broadening at residues 119, 281−283, 323, and 420 (Figure 7a,b). Two of the loops that can contact ligands have low $^{15}N$ $\eta_{xy}$ values at residues 19 and 423 (Figure 7c), suggesting motions within nanoseconds. Thus, $^{15}N$ relaxation suggests internal motions at five of the loops in this cleft where phosphosugars bind.

**Ser108Cys Slowing of Phosphoryl Transfer.** Replacement of Ser108, critical to the phosphoryl transfer reactions of PMM/PGM, with cysteine was investigated for its impact upon catalysis, the structure of the active site, its substrate affinity, and its suitability for ligand binding studies. Even after extensive incubation with G1,6P (the most effective phosphorylating agent for the enzyme), no phosphorylation of PMM/PGM-(S108C) was detected (cf. Figure S3b of the Supporting Information), consistent with removal of the principal acceptor of a phosphoryl group. The apparent $K_m$ for G1P remains similar for the wt and S108C-substituted enzymes (Figure S4 of the Supporting Information), implying a similar affinity for G1P. The mutation was accompanied by a 24-fold lower apparent catalytic turnover ($k_{cat}$) and a 13-fold lower apparent catalytic efficiency ($k_{cat}/K_m$) (Figure S4 of the Supporting Information).

Without the addition of G1,6P, PMM/PGM(S108C) was dramatically slower than the wt enzyme in transforming G1P to G6P, as judged from integrating the anomeric peaks in $^{1}H$ NMR spectra (Figure 8) or $^{13}C$ NMR spectra. Nineteen days and 2 h were required for the mutant enzyme to transform 25% of the glucose phosphate (Figure 8a). In contrast, the wt enzyme generated the same amount of G6P in 88 min, which is 310-fold faster. By completion at 260 min, 2.5% of the initial G1P was transformed into the intermediate G1,6P that had escaped wt PMM/PGM. Addition of G1,6P, which efficiently phosphorylates the wt enzyme but not the S108C mutant enzyme, substantially accelerated the reactions. PMM/PGM-


dx.doi.org/10.1021/bi201609n | *Biochemistry* 2012, 51, 807−819

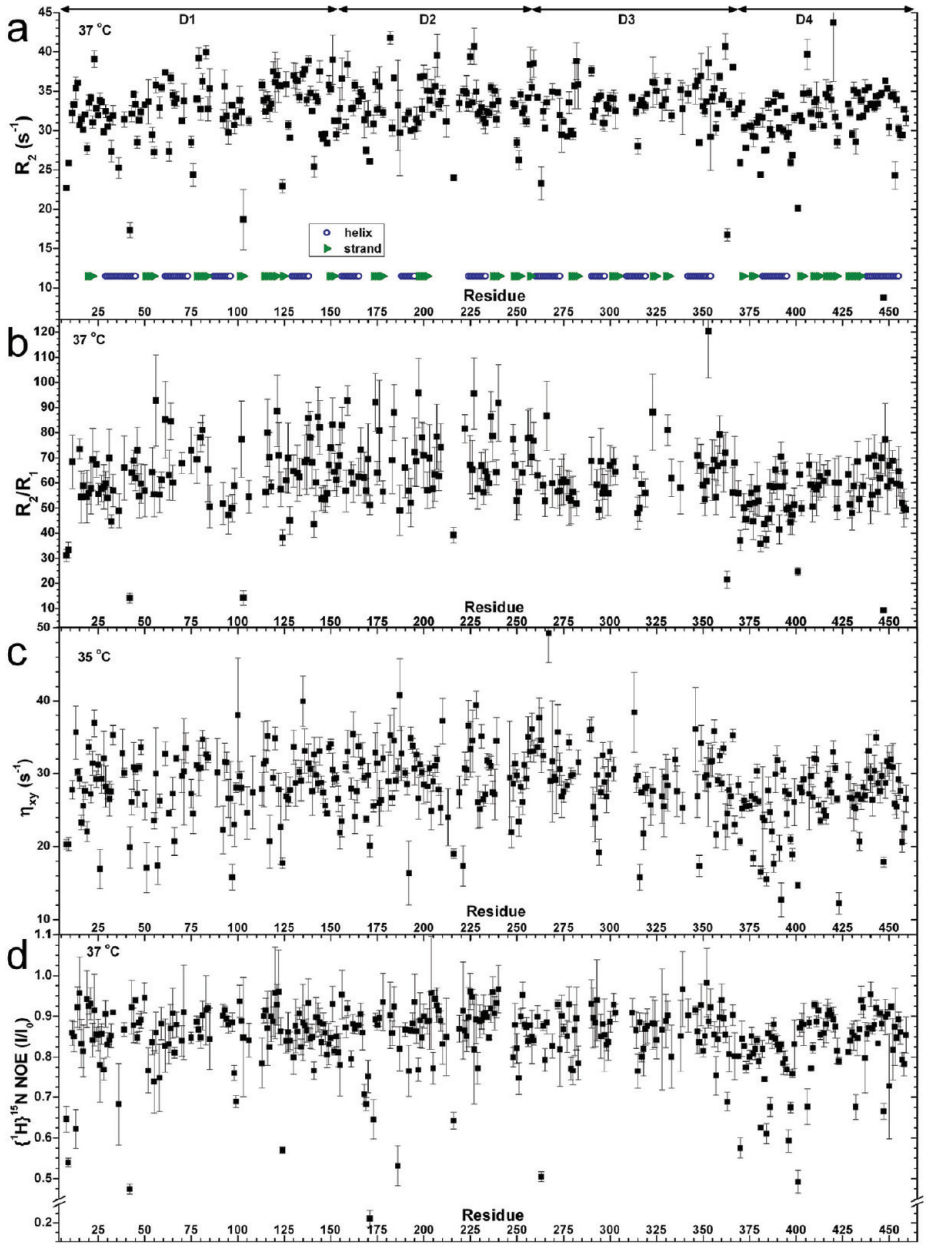


**Figure 7.** $^{15}$N relaxation of wt PMM/PGM recorded at 800 MHz. Shown are $R_2 = 1/T_2$ (a), $R_2/R_1$ (b), transverse cross-correlation rate $\eta_{xy}$ (c), and $\{^1H\}^{15}N$ steady-state NOE difference plotted as $I_{saturated}/I_{nonsaturated}$ (d). The uncertainties in panels a–c are errors in fitting. The uncertainties in panel d are the standard deviations of triplicate measurements.

(S108C) then transformed 25% of the G1P to G6P in ~33 min (Figure 8b), roughly 830-fold faster than without activation. Wild-type and S108C-substituted enzymes transformed 50% of the G1P to G6P in ~7.2 and ~51 min, respectively (Figure 8b). Thus, when G1,6P is present for activation and/or relief of substrate inhibition by G1P, the S108C mutant appeared to be slowed only 7-fold relative to the wt enzyme at high concentrations of G1P and enzyme (Figure 8b). The slowdowns, at both high and low concentrations of the S108C mutant, resemble the 7% level of activity of the previously characterized S108D mutant.[19] Preincubation of PMM/PGM(S108C) with G1,6P for 3.5 h prior to addition of substrate G1P failed to shorten the lag phase. The presence of G1,6P activated wt PMM/PGM by 19-fold, consistent with previous observations of a 20-fold activation by G1,6P.[3] Adding G1,6P (0.7–1.5 $\mu$M) together with a saturating level of G1P activated the S108C mutant at least 40-fold more than the wt enzyme.

**S108C Perturbations of NMR Spectra.** Chemical shift mapping of the effects of the S108C lesion indicated the quarter of backbone peaks most shifted, i.e., those for which $\Delta\omega_{HNC'} \geq 0.062$ ppm, are equally distributed among domains 1–3 (Figure 9a). In contrast, chemical shift perturbations are almost absent from D4. Large peak shifts caused by the S108C mutation (elevated >3$\sigma$) belong to Asp246, which joins Ser108 O$\gamma$ in coordinating the metal, Arg247 and Gly328 each packing with phospho-Ser108, His329 packing with them near the phosphate of Ser108, and Val330 and Phe332 just beyond His329 (Figure 9). A second shell of residues with amide resonances shifted by $\Delta\omega_{HNC'} \geq 0.125$ ppm lie around the bottom of the catalytic cleft, i.e., residues 89, 91, 106, and 117 of D1; 179, 183, 240, 248, and 249 of D2; and 262, 263, 269,


dx.doi.org/10.1021/bi201609n | *Biochemistry* 2012, 51, 807–819

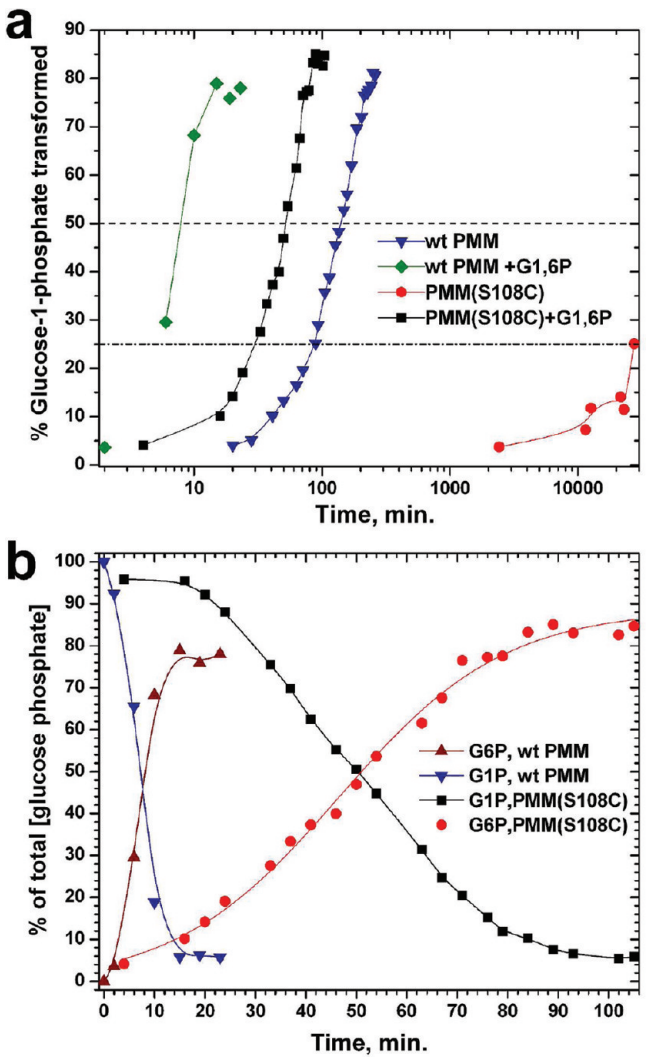


**Figure 8.** Time courses of transformation of G1P by wt and S108C-substituted PMM/PGM, with and without activation by G1,6P. The conditions supported multiple turnovers at 27 °C, pH 7.3, and 33 $\mu$M enzyme. Initial concentrations were 400 $\mu$M G1P and when added 0.66 $\mu$M G1,6P. (a) The transformation of G1P to G6P is represented in the semilog plot. (b) For the G1,6P-activated reactions, the disappearance of G1P and the appearance of G6P (its $\alpha$-anomer) are plotted with an expanded view. The relative concentrations of G1P and G6P were derived by integrating the $^{1}$H NMR peak of the $\alpha$-anomeric proton of each. The finding via $^{13}$C NMR of a 1.67-fold more $\beta$-anomer present was used in determining the total concentration of G6P formed.

281, and 325 of D3 (Figure 9). Accompanying the S108C mutation are cases of smaller NMR peak heights suggestive of line broadening and possible millisecond motion. The following 19 residues within 14 Å of Ser108 (in PDB entry 1K35 of the free state of the wt enzyme) have normalized HNCO peak heights decreased by 40% or more in S108C relative to that in the wt enzyme: 16, 20, 21, 61, 87, 105, 106, 118, 119, 183, 202, 206, 208–210, 246, 248, 307, and 329 (Figure 6). More distant residues with decreased peak heights in the mutant include nine residues in D1, two in D2, five in D3, and two in D4. The decreases could reflect broadening from sampling of alternative conformers or environments (of unknown chemical shift) in milliseconds.

**Effects of the S108C Mutation on the Active Site in the Crystal Structure.** The crystal structure of the apo form of PMM/PGM(S108C) was determined to 2.1 Å (Table 1). Although quite similar to the wt enzyme overall [C$\alpha$ rmsd of 0.39 Å (Figure 10a)], some differences were observed that were unexpected relative to the structures of other mutants at residue 108 (S108D or S108A lesion in PDB entries 2FKF, 2FKM, and 1K2Y)[7,16] and are inconsistent with minimal changes suggested by NMR spectra (Figures 3 and 9a). Poor electron density begins at Cys108 where the side chain could not be modeled and disappears entirely for His109–Tyr114 (Figure 10b). This loop presumably occupies multiple conformations in the crystal of the mutant, leading to the lack of electron density. This result was not anticipated, as cysteine is known to coordinate $Zn^{2+}$ in many proteins. Despite the loss of this side chain interaction, the zinc ion remains bound at full occupancy in the electron density and retains its Asp242, Asp244, and Asp246 ligands (Figure 10b). A phosphate ion, modeled at half-occupancy, fits the electron density and appears to contribute another oxygen ligand for the metal ion but lacks connectivity to any other residues in the protein (Figure 10b). (No phosphate was added during purification but might have originated during protein expression.) Minor perturbations in PMM/PGM(S108C) are small shifts of backbone atoms near His308 at the beginning of a helix abutting the active site (central background of the cleft in Figure 10) and at positions in D4.

In the crystal structure, disordered residues are also present nearby at Tyr17–Leu27 (Figure 10). These regions are linked by hydrogen bonds between the $\beta$-strands from Asp113 to Asn115 and Arg20 to Val23. NMR, however, suggests that both of these $\beta$-strands remain in the S108C mutant enzyme in solution. The SSP values are nearly the same as those of the wt enzyme throughout the entire sequence except for two loops in the active site (Figure 3). $^{13}$C NMR chemical shifts suggest that disorder in solution from the S108C lesion may be confined to the regions of Gly107–Asn110 where peaks could not be assigned and Met104–Thr106 and His329–Phe332 where there are small decreases in the size of SSP values (Figure 3). His329 packs near phospho-Ser108 (Figure 9b). The medium-sized NMR peak shifts induced by the S108C mutation at Gly21, Val23, Tyr114, Phe117, and Lys118 (Figure 9a) lack any significant accompanying change in secondary structure propensity (Figure 3). The CD spectra of wt and S108C mutant enzymes also are very similar (Figure S5 of the Supporting Information). Despite the disorder in the crystal structure where a $\beta$-strand was expected within the region of residues 17–27, spectroscopy suggests the secondary structure in solution to be essentially unaffected outside the immediate vicinity of Cys108.

## DISCUSSION

**Relevance of Domain 4 Mobility to Catalysis.** Previous studies of PMM/PGM have established that the G1,6P (or M1,6P) intermediate must be reoriented by 180° in the active site to regenerate the phospho-enzyme and form the product (Figure 1).[3–5,7] Isotope trapping experiments indicated that the G1,6P intermediate remains associated with the enzyme to form product 14-fold more frequently than it dissociates during a catalytic cycle.[4] Two mutations were found that abolished retention of the intermediate.[7] The mechanism for on-enzyme flipping of the intermediate is an ongoing question about $\alpha$-D-phosphohexomutases.[4,7] Partial opening of the catalytic cleft


dx.doi.org/10.1021/bi201609n | Biochemistry 2012, 51, 807–819

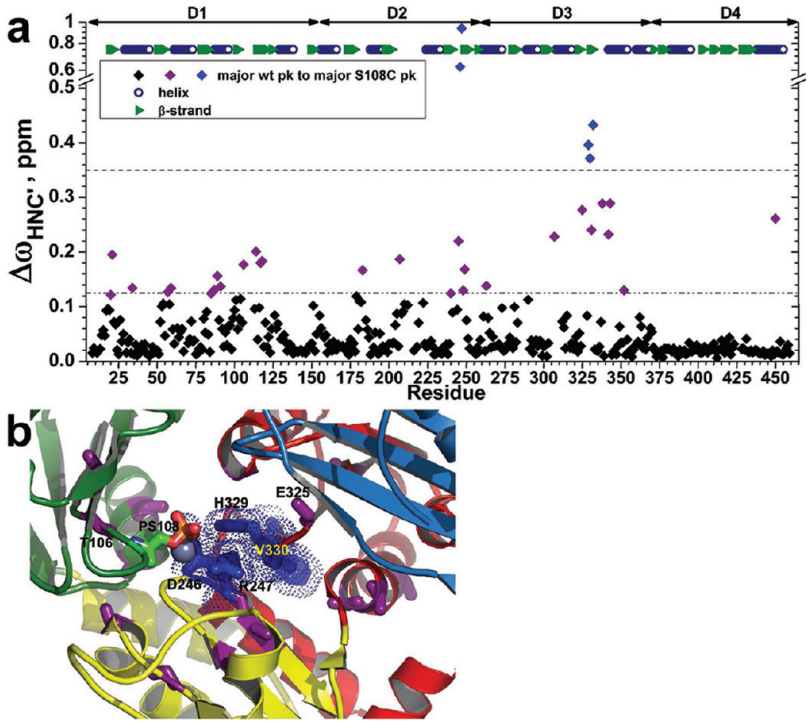


**Figure 9.** Chemical shift perturbations by the S108C mutation. (a) Radial chemical shift changes, calculated as $\Delta\omega_{HNC'} = [(\Delta\omega_{Hn})^2 + (\Delta\omega_N/6)^2 + (\Delta\omega_{C'}/2.4)^2]^{1/2}$, are plotted for each residue's main amide peak in PMM/PGM(S108C) relative to the main peak in the wt enzyme. The peak positions were measured from TROSY-HNCO spectra (800 MHz, 37 °C, and pH 7.4). The larger changes between major peaks in the wt and S108C variants are marked on the crystal structure (PDB entry 1K35) in panel b. Residues with $\Delta\omega_{HNC'} > 0.35$ ppm are colored blue with side chains plotted in panel b. Residues with 0.35 ppm > $\Delta\omega_{HNC'}$ > 0.125 ppm are colored purple with side chains plotted in panel b. Domains 1−4 are colored green, yellow, red, and sky blue, respectively. Phospho-Ser108 is colored by atom type.

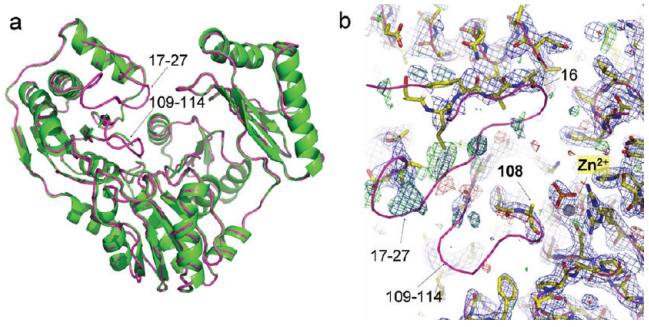


**Figure 10.** Crystal structure of PMM/PGM(S108C). (a) Its backbone ribbon diagram (green) is superimposed on that of the wt enzyme (pink). Disordered segments in D1 are marked with arrows. (b) Electron density maps fitted with yellow sticks show the disordered region of the S108C mutant, again superimposed with the wt structure (pink ribbon) for reference. The $2F_o - F_c$ map is colored blue and contoured at 1.0$\sigma$. The $F_o - F_c$ map is colored green and red and contoured at 3.0$\sigma$ and −3.0$\sigma$, respectively. The metal ion is shown as a gray sphere and the phosphate ion as a stick model.

through rotation of D4 was proposed to facilitate reorientation of the intermediate.[4,7] Association of G1,6P with the phosphate-binding site in D4 was hypothesized to trigger turning of the G1,6P intermediate as D4 rotates.[7] Supporting this suggestion is the half-open cleft observed in the crystal structure with G1,6P bound to phosphorylated PMM/PGM, as well as mutagenesis of Arg421 of the phosphate-binding site in D4.[7] The strongly electropositive field of the active site[16] could retain the bisphosphorylated intermediate when the active site is partly opened for rotation of the intermediate.[7] Rotation of D4 has also been regarded as being pertinent to substrate binding and rate limitation.[4,7]

D4 displays generally greater peak heights in TROSY and triple-resonance spectra and slower $^{15}N$ NMR relaxation compared to D1−D3, both for wt and for S108C-substituted PMM/PGM (Figures 6 and 7). This suggests that the reorientation of D4 as a rigid body is perceptibly faster than that of D1−D3 in the free state of the enzyme in solution. With the X1P inhibitor saturating the active site, detectably higher average peak heights across D4 compared to those across D1−D3 (Figure 6) suggest the possibility that with X1P bound D4 might still reorient slightly more than D1−D3. $^{15}N$ relaxation (Figure 7) suggests the rotations of D4 occur within tens of nanoseconds, based on its rotational correlation time being up to 10% shorter than that of D1−D3 in the free state. This is 4 orders of magnitude faster than the fastest catalytic step, which is completed in 10 ms.[4] Hence, it is possible that many reorientations of D4 can occur within one catalytic cycle. The proposals of mechanistically significant rotations of D4 of PMM/PGM[4,7] are supported by the NMR evidence of the slightly greater mobility of D4 in solution.

What might rigid body rotations of D4 look like? Principal component analysis (PCA) of crystal structures (ranging from open and unbound conformations to closed, ligand-bound states) points out that the most likely mode of rotation of D4 is toward and away from D1, which closes and opens the catalytic cleft (Figure 11a and Movie S1 of the Supporting Information). This large mode (PC1) accounts for ∼82% of the statistical variance among the crystal structures. However, there are two additional modes of conformational change between crystal structures. PC2 is a rotation of D4, relative to D3 (via the

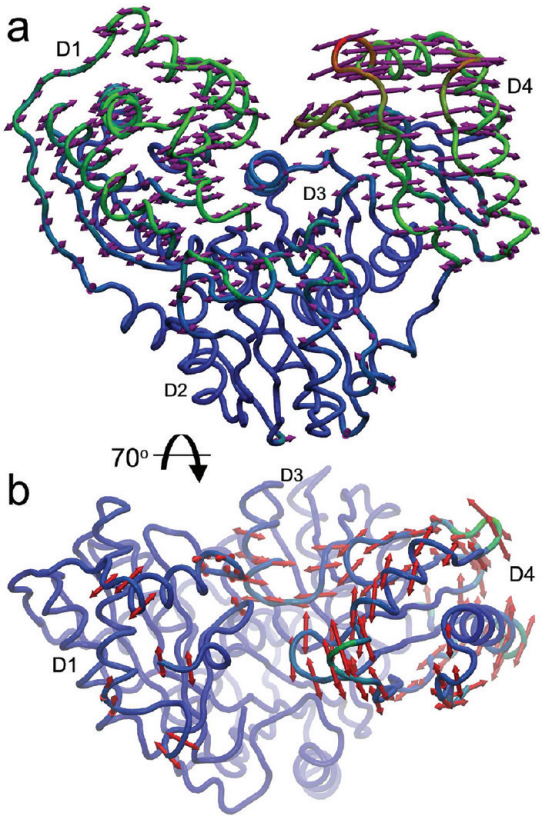


**Figure 11.** Principal component analysis of conformational changes. Principal components 1 and 2 (PC1 and PC2, respectively) from PCA of 12 crystal structures of *P. aeruginosa* PMM/PGM were obtained using ProDy[41] and are depicted on the half-closed conformation bound to the G1,6P intermediate (PDB entry 2FKF). Coloring ranges from blue for minimal rmsd change to green for intermediate change to red for maximal change in Cartesian coordinates. (a) The main rotation (PC1) is D4 toward and away from D1, accompanied by a smaller rotation of D1, as indicated by arrows. This mode accounts for ~82% of the variance among the crystallographic coordinates. (b) The second and orthogonal rotation (PC2), seen from a top view, accounts for ~9% of the variance among the crystal structures. It is largely a rotation of D4 upon D3 underneath, accompanied by limited changes in D1 and D3.

interdomain hinge at Pro368); this accounts for ~9% of the variance among structures (Figure 11b). PC3 is small amplitude rocking of D4 upon D3 in a direction orthogonal to PC1, accounting for ~4% of the structural variance. The narrow interface between D3 and D4 may allow the minor modes of reorientation of D4 relative to D3, i.e., twisting (PC2) or rocking (PC3) of D4. The reorientation of D4 evidently suffices to open the active site cleft enough for reorientation of G16P or M16P for the reaction to proceed (Figure 1).

**Fluctuations in Sugar-Binding Loops.** The hypothesis of millisecond fluctuations among active site loops [suggested by smaller NMR peak heights and their presumed broadening (Figure 6)] is partly supported by faster $^{15}$N relaxation in parts of four of the recognition loops, e.g., those containing Lys117 of D1, Asp283 of D3, the sugar-binding loop (Glu325−His329) of D3, and the phospho-binding loop (Arg421−Ser423) of D4. Broadening of the recognition loop containing Gly307 could instead be attributable to rapid exchange with water (not shown). In various crystal structures, two other recognition loops have multiple or varying conformations and/or side chain disorder at Arg15, Tyr17, Arg20, and Arg247. Changes in the hydrogen bonding of the side chain of Glu325 (from neighboring residues in the free state to interactions with ligands in complexes[45]) are consistent with lower peak heights (Figure 6) and greater $^{15}$N relaxation at this loop (Figure 7b). Intrinsic plasticity in some of the recognition loops might accommodate the adjustments of noncovalent interactions with the substrates, intermediate, and products that were observed in crystal structures of their complexes with PMM/PGM.[5,7]

**Two Sources of Substates.** The correspondence of the minor TROSY peak of 43 residues to the peak observed in the spectra of dephosphorylated wt PMM/PGM (Figure S2b of the Supporting Information) assigns them to the dephosphorylated state. The major and minor peaks of ~72 other residues of the wt enzyme and about 114 residues of intrinsically dephosphorylated PMM/PGM(S108C) presumably arise from some other unidentified source. These latter minor peaks could suggest alternative conformations with a free energy slightly higher than that of the main conformation. Slow conformational fluctuations that overlap on the time scale of milliseconds can be hypothesized for at least 20 amide groups with minor peaks independent of phosphorylation state (Figure S2 of the Supporting Information) and elevated $^{15}$N relaxation rates (Figure 7a,b).

**S108C Defects.** In the absence of G1,6P, PMM/PGM-(S108C) generates G6P from G1P exceedingly slowly (Figure 8a). This contrasts with the generation of G6P by the wt enzyme within a few hundred milliseconds, and maximal release of the G1,6P intermediate in 10 ms.[4] The slow turnover by the S108C mutant cannot be attributed to inferior substrate affinity for PMM/PGM(S108C) because of the similarity of its apparent $K_m$ for G1P to that of the wt enzyme (Figure S4 of the Supporting Information). Upon addition of G1,6P to a reaction mixture, the S108C mutant recovers a significant fraction of wild-type competence in transforming G1P to G6P (Figure 8). This presumably occurs by introducing G1,6P productively to the active site and relieving substrate inhibition. Substrate inhibition by G1P might possibly be enhanced in PMM/PGM(S108C) by its approximately 2-fold greater apparent affinity for G1P (Figure S4 of the Supporting Information). Nonetheless, G1,6P still seems to compete favorably with G1P like it does in the wt enzyme (Figure 8a). Thus, it appears that a catalytic rate limitation must account for the 310-fold reduction in the level of generation of G6P in the absence of G1,6P. This could result from the lack of phosphorylation of the mutant enzyme. Because preincubation of PMM/PGM(S108C) with G1,6P failed either to lead to accumulation of detectable phosphorylation or to shorten reaction lag phase (compared to adding it at the start of the reaction), any phosphorylation of the mutant enzyme is not faster than its dephosphorylation. The addition of G1,6P might slightly or transiently phosphorylate an alternative side chain (possibly even Cys108) to an experimentally undetectable level, but sufficient for the activity observed to be 7−30-fold slower than that of the wild type (Figure 7 and Figure S4 of the Supporting Information). Alternative side chains for phosphoryl transfer were considered without finding a single essential residue.[19] The similarly impaired conversion of G1P to G6P by S108A and S108D mutants[19] suggests that they share the same bottleneck.

Though the electron density for residues 17−27 and 113−115 is lost in the crystal of PMM/PGM(S108C) (Figure 10) and chemical shift perturbations of ~0.2 ppm occur at the two

β-strands therein (Figure 9a), their NMR secondary structure propensities remain virtually unchanged (Figure 3). This suggests little consequence of the mutation on either the loops or β-strands therein (Ile19−Val22 and Tyr114−Val121) in solution. The chemical shift perturbations (Figure 9a) and small changes to secondary structure propensities (Figure 3) agree upon a small effect of the S108C mutation on the nearby sugar-binding loop (Glu325−His329) in solution. However, these and the other small to medium-sized chemical shift changes surrounding the bottom of the active site in D1−D3 (purple in Figure 9b) are not accompanied by corresponding changes in the crystal structure, suggesting only subtle effects in solution.

Higher NMR peak heights of D4 in the X1P inhibitor complex with the S108C-substituted enzyme (Figure 6) raise the question of whether D4 in this complex retains slightly greater freedom in solution. If so, this could be consistent with the widening of the cleft observed in the crystal structure of the S108A mutant.[16] The possibility of the loosening of conformational restraints on D4 via the removal of phospho-Ser108 might be due to the loss of its electrostatic attraction for the nearest positive charges in D4 (Arg421, Arg432, and Lys385).

**Summary.** The NMR characterization of multidomain PMM/PGM is opening opportunities for studying the functional interplay among its domains in solution, vis-à-vis well-established results from crystallography and enzymology. Insights from solution NMR and crystallography are proving to be complementary for this system. While the S108C mutation is accompanied by disorder of residues 17−27 in the crystallographic electron density, NMR suggests the β-strand and flanking loops therein probably remain unchanged in solution. In contrast, NMR detects small perturbations of the peaks of domains 2 and 3 in the S108C mutant, despite no apparent changes there in the crystal structure. Catalysis impaired by the S108C lesion could simplify future investigations of substrate−product binding conducted in the absence of the G1,6P activator. NMR reveals the presence of different states of the enzyme, including phosphorylated and dephosphorylated forms, affecting a quarter or more of the backbone. $^{15}$N NMR relaxation and peak heights are suggestive of (a) slightly greater and different rotational diffusion of domain 4, possibly detectable even with an inhibitor bound, and (b) millisecond fluctuations affecting at least four ligand-binding loops around the active site. This is consistent with the conformational variability of this domain observed from crystal structures. The lines of evidence for the slightly independent mobility of domain 4 in solution corroborate the working hypothesis that rotation of domain 4 is important to the multistep catalysis of PMM/PGM,[7] a promising topic for further investigation.

## ■ ASSOCIATED CONTENT

### Supporting Information

Examples of major and minor amide NMR peaks (Figure S1), chemical shift differences between major and minor peaks and between dephosphorylated and phosphorylated enzymes (Figure S2), mass spectra (Figure S3), steady-state enzyme kinetics of wt and S108C-substituted PMM (Figure S4), similarity of CD spectra of wt and S108C mutant enzymes (Figure S5), $^{15}$N $\eta_{xy}$ relaxation of PMM/PGM(S108C) (Figure S6), diffusion tensors of D1−D3 and D4 (Figure S7), and crystallographic range of opening of the catalytic cleft derived using PCA (Movie S1). This material is available free of charge via the Internet at http://pubs.acs.org.

### Accession Codes

The NMR peak assignments have been deposited in the BioMagResBank as entry 17602 for major and minor peaks of wt PMM/PGM and entry 17652 for PMM/PGM(S108C). The coordinates of PMM/PGM(S108C) have been deposited as PDB entry 3RSM.

## ■ AUTHOR INFORMATION


### Corresponding Author

*E-mail: vandorens@missouri.edu (S.R.V.D.) or beamerl@missouri.edu (L.J.B.). Phone: (573) 882-5113. Fax: (573) 882-5635.

### Present Addresses

†Shankel Structural Biology Center, University of Kansas, Lawrence, KS 66047.

‡Department of Computing Science, University of Alberta, Edmonton, AB, Canada T6G 2E8.



### Funding

Grants from the National Science Foundation (MCB 0918389), the National Institutes of Health (R03AI074779), and the University of Missouri Research Board supported this work. The University of Missouri and National Institutes of Health Grant RR022341 generously supported acquisition of the 800 MHz NMR spectrometer.


## ■ ACKNOWLEDGMENTS


Dale Karr and Andrew Schramm provided support for protein preparation. Prof. Tom Mawhinney synthesized the xylose 1-phosphate. We thank Prof. Cristina Furdui for discussion of enzyme kinetics results and Dr. Beverly Dague of the Gehrke Proteomics Center for mass spectra.


## ■ ABBREVIATIONS

CD, circular dichroism; D1−D4, domains 1−4, respectively; DD-CSA, dipole−dipole/chemical shift anisotropy; GS, generic spin system; G1P, glucose 1-phosphate; G1,6P, glucose 1,6-bisphosphate; G6P, glucose 6-phosphate; LPS, lipopolysaccharide; M1,6P, mannose 1,6-bisphosphate; PCA, principal component analysis; PMM/PGM or PMM, phosphomannomutase/phosphoglucomutase; SSP, secondary structure propensity; TROSY, transverse relaxation-optimized spectroscopy; wt, wild-type; X1P, xylose 1-phosphate.

## ■ REFERENCES


(1) Ray, W. J. Jr., and Roscelli, G. A. (1964) A Kinetic Study of the Phosphoglucomutase Pathway. *J. Biol. Chem. 239*, 1228−1236.

(2) Shackelford, G. S., Regni, C. A., and Beamer, L. J. (2004) Evolutionary trace analysis of the α-D-phosphohexomutase superfamily. *Protein Sci. 13*, 2130−2138.

(3) Naught, L. E., and Tipton, P. A. (2001) Kinetic Mechanism and pH Dependence of the Kinetic Parameters of *Pseudomonas aeruginosa* Phosphomannomutase/Phosphoglucomutase. *Arch. Biochem. Biophys. 396*, 111−118.

(4) Naught, L. E., and Tipton, P. A. (2005) Formation and reorientation of glucose 1,6-bisphosphate in the PMM/PGM reaction: Transient-state kinetic studies. *Biochemistry 44*, 6831−6836.

(5) Regni, C., Naught, L. E., Tipton, P. A., and Beamer, L. J. (2004) Structural basis of diverse substrate recognition by the enzyme PMM/PGM from *P. aeruginosa*. *Structure 12*, 55−63.

(6) Ye, R. W., Zielinski, N. A., and Chakrabarty, A. M. (1994) Purification and characterization of phosphomannomutase/phospho-

glucomutase from *Pseudomonas aeruginosa* involved in biosynthesis of both alginate and lipopolysaccharide. *J. Bacteriol. 176*, 4851−4857.
(7) Regni, C., Schramm, A. M., and Beamer, L. J. (2006) The Reaction of Phosphohexomutase from *Pseudomonas aeruginosa*: Structural Insights into a Simple Processive Enzyme. *J. Biol. Chem. 281*, 15564−15571.
(8) King, J. D., Kocíncová, D., Westman, E. L., and Lam, J. S. (2009) Review: Lipopolysaccharide biosynthesis in *Pseudomonas aeruginosa*. *Innate Immun. 15*, 261−312.
(9) Olvera, C., Goldberg, J. B., Sanchez, R., and Soberon-Chavez, G. (1999) The *Pseudomonas aeruginosa algC* gene product participates in rhamnolipid biosynthesis. *FEMS Microbiol. Lett. 179*, 85−90.
(10) Rocchetta, H. L., Pacan, J. C., and Lam, J. S. (1998) Synthesis of the A-band polysaccharide sugar D-rhamnose requires Rmd and WbpW: Identification of multiple AlgA homologues, WbpW and ORF488, in *Pseudomonas aeruginosa*. *Mol. Microbiol. 29*, 397−398.
(11) Remminghorst, U., and Rehm, B. H. (2006) Bacterial alginates: From biosynthesis to applications. *Biotechnol. Lett. 28*, 1701−1712.
(12) Hentzer, M., Teitzel, G. M., Balzer, G. J., Heydorn, A., Molin, S., Givskov, M., and Parsek, M. R. (2001) Alginate Overproduction Affects *Pseudomonas aeruginosa* Biofilm Structure and Function. *J. Bacteriol. 183*, 5395−5401.
(13) Govan, J. R. W., and Deretic, V. (1996) Microbial pathogenesis in cystic fibrosis: Mucoid *Pseudomonas aeruginosa* and *Burkholderia cepacia*. *Microbiol. Rev. 60*, 539−574.
(14) Li, X. J., Li, Q., Si, L. Y., and Yuan, Q. Y. (2011) Bacteriological Differences Between Patients with Acute Exacerbation of COPD and Community-Acquired Pneumonia. *Respiratory Care 56*, doi: 10.4187/respcare.00915.
(15) Lowry, O. H., and Passonneau, J. V. (1969) Phosphoglucomutase kinetics with the phosphates of fructose, glucose, mannose, ribose, and galactose. *J. Biol. Chem. 244*, 910−916.
(16) Regni, C., Tipton, P. A., and Beamer, L. J. (2002) Crystal structure of PMM/PGM: An enzyme in the biosynthetic pathway of *P. aeruginosa* virulence factors. *Structure 10*, 269−279.
(17) Murzin, A. G., Brenner, S. E., Hubbard, T., and Chothia, C. (1995) SCOP: A structural classification of proteins database for the investigation of sequences and structures. *J. Mol. Biol. 247*, 536−540.
(18) Regni, C., Shackelford, G. S., and Beamer, L. J. (2006) Complexes of the enzyme phosphomannomutase/phosphoglucomutase with a slow substrate and an inhibitor. *Acta Crystallogr. F62*, 722−726.
(19) Naught, L. E., Regni, C., Beamer, L. J., and Tipton, P. A. (2003) Roles of active site residues in *P. aeruginosa* phosphomannomutase/phosphoglucomutase. *Biochemistry 42*, 9946−9951.
(20) Riek, R., Pervushin, K., and Wuthrich, K. (2000) TROSY and CRINEPT: NMR with large molecular and supramolecular structures in solution. *Trends Biochem. Sci. 25*, 462−468.
(21) Salzmann, M., Pervushin, K., Wider, G., Senn, H., and Wuthrich, K. (1998) TROSY in triple-resonance experiments: New perspectives for sequential NMR assignment of large proteins. *Proc. Natl. Acad. Sci. U.S.A. 95*, 13585−13590.
(22) Tugarinov, V., Muhandiram, R., Ayed, A., and Kay, L. E. (2002) Four-dimensional NMR spectroscopy of a 723-residue protein: Chemical shift assignments and secondary structure of malate synthase G. *J. Am. Chem. Soc. 124*, 10025−10035.
(23) Edison, A. S., Abildgaard, F., Westler, W. M., Mooberry, E. S., and Markley, J. L. (1994) Practical Introduction to Theory and Implementation of Multinuclear, Multidimensional Nuclear Magnetic Resonance Experiments. *Methods Enzymol. 239*, 3−79.
(24) Delaglio, F., Grzesiek, S., Vuister, G. W., Zhu, G., Pfeifer, J., and Bax, A. (1995) NMRPipe: A multidimensional spectral processing system based on UNIX pipes. *J. Biomol. NMR 6*, 277−293.
(25) Goddard, T. D., and Kneller, D. G. (2000) *SPARKY*, University of California, San Francisco.
(26) Grzesiek, S., and Bax, A. (1993) Amino acid type determination in the sequential assignment procedure of uniformly $^{13}C/^{15}N$-enriched proteins. *J. Biomol. NMR 3*, 185−204.
(27) Jung, Y. S., and Zweckstetter, M. (2004) Mars: Robust automatic backbone assignment of proteins. *J. Biomol. NMR 30*, 11−23.
(28) Crippen, G., Rousaki, A., Revington, M., Zhang, Y., and Zuiderweg, E. (2010) SAGA: Rapid automatic mainchain NMR assignment for large proteins. *J. Biomol. NMR 46*, 281−298.
(29) Marsh, J. A., Singh, V. K., Jia, Z., and Forman-Kay, J. D. (2006) Sensitivity of secondary structure propensities to sequence differences between $\alpha$- and $\gamma$-synuclein: Implications for fibrillation. *Protein Sci. 15*, 2795−2804.
(30) Wishart, D. S., Arndt, D., Berjanskii, M., Tang, P., Zhou, J., and Lin, G. (2008) CS23D: A web server for rapid protein structure generation using NMR chemical shifts and sequence data. *Nucleic Acids Res. 36*, W496−W502.
(31) Zhu, G., Xia, Y., Nicholson, L. K., and Sze, K. H. (2000) Protein Dynamics Measurements by TROSY-Based NMR Experiments. *J. Magn. Reson. 143*, 423−426.
(32) Liu, Y., and Prestegard, J. H. (2008) Direct measurement of dipole-dipole/CSA cross-correlated relaxation by a constant-time experiment. *J. Magn. Reson. 193*, 23−31.
(33) Fushman, D., Weisemann, R., Thüring, H., and Rüterjans, H. (1994) Backbone dynamics of ribonuclease T1 and its complex with 2′GMP studied by two-dimensional heteronuclear NMR spectroscopy. *J. Biomol. NMR 4*, 61−78.
(34) Lee, D., Hilty, C., Wider, G., and Wüthrich, K. (2006) Effective rotational correlation times of proteins from NMR relaxation interference. *J. Magn. Reson. 178*, 72−76.
(35) Dosset, P., Hus, J. C., Blackledge, M., and Marion, D. (2000) Efficient analysis of macromolecular rotational diffusion from heteronuclear relaxation data. *J. Biomol. NMR 16*, 23−28.
(36) Regni, C. A., Tipton, P. A., and Beamer, L. J. (2000) Crystallization and initial crystallographic analysis of phosphomannomutase/phosphoglucomutase from *Pseudomonas aeruginosa*. *Acta Crystallogr. D56*, 761−762.
(37) Pflugrath, J. (1999) The finer things in X-ray diffraction data collection. *Acta Crystallogr. D55*, 1718−1725.
(38) Murshudov, G. N., Vagin, A. A., Lebedev, A., Wilson, K. S., and Dodson, E. J. (1999) Efficient anisotropic refinement of macromolecular structures using FFT. *Acta Crystallogr. D55*, 247−255.
(39) Emsley, P., and Cowtan, K. (2004) Coot: Model-building tools for molecular graphics. *Acta Crystallogr. D60*, 2126−2132.
(40) Bakan, A., and Bahar, I. (2009) The intrinsic dynamics of enzymes plays a dominant role in determining the structural changes induced upon inhibitor binding. *Proc. Natl. Acad. Sci. U.S.A. 106*, 14349−14354.
(41) Bakan, A., Meireles, L. M., and Bahar, I. (2011) ProDy: Protein Dynamics Inferred from Theory and Experiments. *Bioinformatics*, doi: 10.1093/bioinformatics/btr168.
(42) Revington, M., and Zuiderweg, E. R. (2004) TROSY-driven NMR backbone assignments of the 381-residue nucleotide-binding domain of the *Thermus thermophilus* DnaK molecular chaperone. *J. Biomol. NMR 30*, 113−114.
(43) Aurora, R., and Rose, G. D. (1998) Helix capping. *Protein Sci. 7*, 21−38.
(44) Bertelsen, E. B., Chang, L., Gestwicki, J. E., and Zuiderweg, E. R. P. (2009) Solution conformation of wild-type *E. coli* Hsp70 (DnaK) chaperone complexed with ADP and substrate. *Proc. Natl. Acad. Sci. U.S.A. 106*, 8471−8476.
(45) Schramm, A. M., Mehra-Chaudhary, R., Furdui, C. M., and Beamer, L. J. (2008) Backbone flexibility, conformational change, and catalysis in a phosphohexomutase from *Pseudomonas aeruginosa*. *Biochemistry 47*, 9154−9162.